Anal. Chem. **2007,** *79,* 523−532

Atmospheric Pressure Molecular Imaging by Infrared MALDI Mass Spectrometry

Yue Li, Bindesh Shrestha, and Akos Vertes*

Department of Chemistry, Institute for Proteomics Technology and Applications, George Washington University, Washington, DC 20052

An atmospheric pressure (AP) MALDI imaging interface was developed for an orthogonal acceleration time-of-flight mass spectrometer and utilized to analyze peptides, carbohydrates, and other small biomolecules using infrared laser excitation. In molecular imaging experiments, the spatial distribution of mock peptide patterns was recovered with a detection limit of ~1 fmol/pixel from a variety of MALDI matrixes. With the use of oversampling for the image acquisition, a spatial resolution of 40 μm, 5 times smaller than the laser spot size, was achieved. This approach, however, required that the analyte was largely removed at the point of analysis before the next point was interrogated. Native water in plant tissue was demonstrated to be an efficient natural matrix for AP infrared laser desorption ionization. In soft fruit tissues from bananas, grapes, and strawberries, potassiated ions of the most abundant metabolites, small carbohydrates, and their clusters produced the strongest peaks in the spectra. Molecular imaging of a strawberry skin sample revealed the distribution of the sucrose, glucose/fructose, and citric acid species around the embedded seeds. Infrared AP MALDI mass spectrometric imaging without the addition of an artificial matrix enables the in vivo investigation of small biomolecules and biological processes (e.g., metabolomics) in their natural environment.

Molecular imaging with mass spectrometry (MS) has attracted the attention of scientists for over 3 decades because it offers the benefit of excellent sensitivity combined with the ability to uniquely identify an array of chemical species in the image. The top contenders to deliver on this promise are secondary ion mass spectrometry (SIMS) and matrix-assisted laser desorption ionization (MALDI). Excellent recent reviews on the development and application of these methods are available in the literature.[1−5] In many respects the two techniques are complementary. For example, SIMS produces high lateral resolution (<20 nm) distributions of elemental and small organic ions (m/z < 1000), whereas MALDI-MS imaging using an ultraviolet (UV) laser reports on larger species (1000 < m/z < 50 000 for proteins) with coarser resolution (typically 30−200 μm). The demonstrated ability of MALDI-MS imaging to reveal protein distributions in tissue sections[6] resulted in heightened interest and the rapid growth of related publications during the past 5 years.[7−20]

Tissue sections are prepared for MALDI imaging by uniformly covering the surface with matrix solution. An alternative method is to blot the species of interest onto the target followed by the application of matrix. Although necessary, these steps, perhaps, are the most critical, as the analyzed species have to be transferred into the matrix overlayer without significant degradation of its lateral distribution by diffusion and/or mixing. After air-drying, the treated sample is transferred into the vacuum system of the mass spectrometer where an automated $X-Y$ stage moves the sample in the laser desorption ion source. By synchronizing the target movement to the ultraviolet laser shots, spatially correlated mass spectra are acquired.

Application of MALDI imaging to large biomolecules critically depends on sample preparation. Depending on crystallization conditions a layer of more or less fine crystallites of the UV matrix

* To whom correspondence should be addressed. vertes@gwu.edu.

(1) Pacholski, M. L.; Winograd, N. *Chem. Rev.* **1999**, *99*, 2977−3005.
(2) Todd, P. J.; Schaaff, T. G.; Chaurand, P.; Caprioli, R. M. *J. Mass Spectrom.* **2001**, *36*, 355−369.
(3) McPhail, D. S. *J. Mater. Sci.* **2006**, *41*, 873−903.
(4) Rubakhin, S. S.; Jurchen, J. C.; Monroe, E. B.; Sweedler, J. V. *Drug Discovery Today* **2005**, *10*, 823−837.
(5) Caldwell, R. L.; Caprioli, R. M. *Mol. Cell. Proteomics* **2005**, *4*, 394−401.
(6) Stoeckli, M.; Chaurand, P.; Hallahan, D. E.; Caprioli, R. M. *Nat. Med.* **2001**, *7*, 493−496.
(7) Hsieh, Y.; Casale, R.; Fukuda, E.; Chen, J. W.; Knemeyer, I.; Wingate, J.; Morrison, R.; Korfmacher, W. *Rapid Commun. Mass Spectrom.* **2006**, *20*, 965−972.
(8) Altelaar, A. F. M.; Klinkert, I.; Jalink, K.; de Lange, R. P. J.; Adan, R. A. H.; Heeren, R. M. A.; Piersma, S. R. *Anal. Chem.* **2006**, *78*, 734−742.
(9) Wang, H. Y. J.; Jackson, S. N.; McEuen, J.; Woods, A. S. *Anal. Chem.* **2005**, *77*, 6682−6686.
(10) Rohner, T. C.; Staab, D.; Stoeckli, M. *Mech. Ageing Dev.* **2005**, *126*, 177−185.
(11) Maddalo, G.; Petrucci, F.; Iezzi, M.; Pannellini, T.; Del Boccio, P.; Ciavardelli, D.; Biroccio, A.; Forli, F.; Di Ilio, C.; Ballone, E.; Urbani, A.; Federici, G. *Clin. Chim. Acta* **2005**, *357*, 210−218.
(12) Crecelius, A. C.; Cornett, D. S.; Caprioli, R. M.; Williams, B.; Dawant, B. M.; Bodenheimer, B. *J. Am. Soc. Mass Spectrom.* **2005**, *16*, 1093−1099.
(13) Touboul, D.; Piednoel, H.; Voisin, V.; De La Porte, S.; Brunelle, A.; Halgand, F.; Laprevote, O. *Eur. J. Mass Spectrom.* **2004**, *10*, 657−664.
(14) Luxembourg, S. L.; Mize, T. H.; McDonnell, L. A.; Heeren, R. M. A. *Anal. Chem.* **2004**, *76*, 5339−5344.
(15) Brunelle, A.; Touboul, D.; Piednoel, H.; Voisin, V.; De La Porte, S.; Tallarek, E.; Hagenhoff, B.; Halgand, F.; Laprevote, O. *Mol. Biol. Cell* **2004**, *15*, 103A−104A.
(16) Reyzer, M. L.; Hsieh, Y. S.; Ng, K.; Korfmacher, W. A.; Caprioli, R. M. *J. Mass Spectrom.* **2003**, *38*, 1081−1092.
(17) Kruse, R.; Sweedler, J. V. *J. Am. Soc. Mass Spectrom.* **2003**, *14*, 752−759.
(18) Chaurand, P.; Fouchecourt, S.; DaGue, B. B.; Xu, B. G. J.; Reyzer, M. L.; Orgebin-Crist, M. C.; Caprioli, R. M. *Proteomics* **2003**, *3*, 2221−2239.
(19) Spengler, B.; Hubert, M. *J. Am. Soc. Mass Spectrom.* **2002**, *13*, 735−748.
(20) Chaurand, P.; Schwartz, S. A.; Caprioli, R. M. *Curr. Opin. Chem. Biol.* **2002**, *6*, 676−681.

10.1021/ac061577n CCC: $37.00
Published on Web 12/13/2006

is formed over the biological material. During their formation, these crystallites incorporate some of the proteins from the tissue section.[6,21−26] This approach has been successfully used to profile and image peptides and proteins from mammalian cells and tissue sections[20] including samples from colon tumors.[27]

There are significant efforts underway to refine molecular imaging methods based on MALDI-MS technology.[5,8,12,14,19,20,28−35] Recent advances in instrumentation pioneered on a home-built system promise close to diffraction-limited lateral resolution (0.6 μm for $\lambda = 337$ nm laser wavelength), rapid image collection (up to 50 pixels per second), and the combination of MALDI imaging with confocal microscopy.[19] With the use of a high repetition rate (8 kHz) Nd:YLF laser and a fast piezoelectric nanostage a 100 × 100 pixel image can be acquired within 4−15 min. On this system, inorganic ion distributions in pine tree root tissue sections were recorded with excellent spatial resolution.

Probing the surface point by point has two important disadvantages. First, it is inherently slow due to the limitations in the rate of laser pulses and/or data acquisition. Second, the above-mentioned diffraction-limited focusing reduces the spatial resolution. Both of these obstacles can be resolved by switching to the "microscope mode" known from SIMS imaging.[14,32] In this mode the highly focused laser beam is replaced by large area illumination and spatially resolved ion detection. In a single shot experiment mass-resolved images are obtained for the intact peptide and protein ions of a 200 μm spot with a spatial resolution of 4 μm in less than 1 ms. This powerful approach, however, can only be applied in a vacuum environment for at atmospheric pressure the congruence of ion trajectories is spoiled by the collisions of the ions with the background gas molecules.

Although the feasibility of atmospheric pressure (AP) MALDI has been demonstrated several years ago,[36−42] its analytical applications are just beginning to emerge.[43−45] Initially the enthusiasm was tempered by its reduced sensitivity compared to that of vacuum MALDI, but the recently reported subfemtomole detection limits (in combination with preconcentration methods, e.g., solid-phase microextraction) and the streamlined sample handling in the ambient rekindled the interest.[46] Additional advantages of AP-MALDI include the possibility to use liquid matrixes and, in combination with a mid-IR laser, to efficiently study carbohydrates, their complexes, and noncovalent peptide−carbohydrate interactions.[47−50]

Conventional MALDI-MS relies on a UV laser to produce the ions. Although infrared (IR) MALDI had been demonstrated to produce intact ions of large nucleic acids and work with water ice as a matrix,[51,52] due to its less robust analytical performance compared to that of UV-MALDI and to the lack of inexpensive mid-IR laser sources it was not universally embraced by the analytical community. Nevertheless, the inherent advantages of IR-MALDI for certain applications are compelling. Direct combination of IR-MALDI with liquid-phase separation techniques[53−56] and with thin-layer chromatography[57] have been demonstrated in the literature. There are also more potential matrixes for IR-MALDI because many compounds have a strong absorption in the mid-IR spectral region. Recently, Laiko et al.[58] successfully used water and glycerol as a matrix with a 3 μm IR laser at atmospheric pressure to generate peptide ions.

An important figure of merit for imaging techniques is their spatial resolution. In its current form, MALDI-MS imaging is performed in the scanning microprobe mode. In this approach, the focal spot of the laser beam coincides with the sampling volume of the mass spectrometer and the sample is scanned by

(21) Koomen, J. M.; Russell, D. H. *J. Mass Spectrom.* **2000**, *35*, 1025−1034.
(22) Chaurand, P.; Stoeckli, M.; Caprioli, R. M. *Anal. Chem.* **1999**, *71*, 5263−5270.
(23) Zhang, H.; Stoeckli, M.; Andren, P. E.; Caprioli, R. M. *J. Mass Spectrom.* **1999**, *34*, 377−383.
(24) Stoeckli, M.; Farmer, T. B.; Caprioli, R. M. *J. Am. Soc. Mass Spectrom.* **1999**, *10*, 67−71.
(25) Chaurand, P.; Caprioli, R. M. *Electrophoresis* **2002**, *23*, 3125−3135.
(26) Caprioli, R. M.; Farmer, T. B.; Gile, J. *Anal. Chem.* **1997**, *69*, 4751−4760.
(27) Chaurand, P.; DaGue, B. B.; Pearsall, R. S.; Threadgill, D. W.; Caprioli, R. M. *Proteomics* **2001**, *1*, 1320−1326.
(28) Luxembourg, S. L.; McDonnell, L. A.; Duursma, M. C.; Guo, X. H.; Heeren, R. M. A. *Anal. Chem.* **2003**, *75*, 2333−2341.
(29) Altelaar, A. F. M.; van Minnen, J.; Jimenez, C. R.; Heeren, R. M. A.; Piersma, S. R. *Anal. Chem.* **2005**, *77*, 735−741.
(30) James, A.; Dindyal-Popescu, A.; Scott, G.; Zhao, J. Y. *Clin. Chem.* **2005**, *51*, A204−A205.
(31) Jurchen, J. C.; Rubakhin, S. S.; Sweedler, J. V. *J. Am. Soc. Mass Spectrom.* **2005**, *16*, 1654−1659.
(32) Luxembourg, S. L.; McDonnell, L. A.; Mize, T. H.; Heeren, R. M. A. *J. Proteome Res.* **2005**, *4*, 671−673.
(33) McCombie, G.; Staab, D.; Stoeckli, M.; Knochenmuss, R. *Anal. Chem.* **2005**, *77*, 6118−6124.
(34) Crossman, L.; McHugh, N. A.; Hsieh, Y. S.; Korfmacher, W. A.; Chen, J. W. *Rapid Commun. Mass Spectrom.* **2006**, *20*, 284−290.
(35) Lemaire, R.; Tabet, J. C.; Ducoroy, P.; Hendra, J. B.; Salzet, M.; Fournier, I. *Anal. Chem.* **2006**, *78*, 809−819.
(36) Laiko, V. V.; Baldwin, M. A.; Burlingame, A. L. *Anal. Chem.* **2000**, *72*, 652−657.
(37) Galicia, M. C.; Vertes, A.; Callahan, J. H. *Anal. Chem.* **2002**, *74*, 1891−1895.
(38) Doroshenko, V. M.; Laiko, V. V.; Taranenko, N. I.; Berkout, V. D.; Lee, H. S. *J. Int. Mass Spectrom.* **2002**, *221*, 39−58.
(39) Callahan, J. H.; Galicia, M. C.; Vertes, A. *Appl. Surf. Sci.* **2002**, *197*, 130−137.
(40) Laiko, V. V.; Moyer, S. C.; Cotter, R. J. *Anal. Chem.* **2000**, *72*, 5239−5243.
(41) Moyer, S. C.; Cotter, R. J.; Woods, A. S. *J. Am. Soc. Mass Spectrom.* **2002**, *13*, 274−283.
(42) Moyer, S. G.; Cotter, R. J. *Anal. Chem.* **2002**, *74*, 468A−476A.
(43) Zhang, J. H.; LaMotte, L. T.; Dodds, E. D.; Lebrilla, C. B. *Anal. Chem.* **2005**, *77*, 4429−4438.
(44) Hanton, S. D.; Parees, D. M.; Zweigenbaum, J. *J. Am. Soc. Mass Spectrom.* **2006**, *17*, 453−458.
(45) Creaser, C. S.; Ratcliffe, L. *Curr. Anal. Chem.* **2006**, *2*, 9−15.
(46) Wang, Y.; Schneider, B. B.; Covey, T. R.; Pawliszyn, J. *Anal. Chem.* **2005**, *77*, 8095−8101.
(47) Von Seggern, C. E.; Cotter, R. J. *J. Mass Spectrom.* **2004**, *39*, 736−742.
(48) Von Seggern, C. E.; Moyer, S. C.; Cotter, R. J. *Anal. Chem.* **2003**, *75*, 3212−3218.
(49) Von Seggern, C. E.; Zarek, P. E.; Cotter, R. J. *Anal. Chem.* **2003**, *75*, 6523−6530.
(50) Tan, P. V.; Taranenko, N. I.; Laiko, V. V.; Yakshin, M. A.; Prasad, C. R.; Doroshenko, V. M. *J. Mass Spectrom.* **2004**, *39*, 913−921.
(51) Berkenkamp, S.; Kirpekar, F.; Hillenkamp, F. *Science* **1998**, *281*, 260−262.
(52) Berkenkamp, S.; Karas, M.; Hillenkamp, F. *Proc. Natl. Acad. Sci. U.S.A.* **1996**, *93*, 7003−7007.
(53) Daniel, J. M.; Laiko, V. V.; Doroshenko, V. M.; Zenobi, R. *Anal. Bioanal. Chem.* **2005**, *383*, 895−902.
(54) Daniel, J. M.; Ehala, S.; Friess, S. D.; Zenobi, R. *Analyst* **2004**, *129*, 574−578.
(55) Xu, Y. C.; Little, M. W.; Murray, K. K. *J. Am. Soc. Mass Spectrom.* **2006**, *17*, 469−474.
(56) Lawson, S. J.; Murray, K. K. *Rapid Commun. Mass Spectrom.* **2000**, *14*, 129−134.
(57) Dreisewerd, K.; Kolbl, S.; Peter-Katalinic, J.; Berkenkamp, S.; Pohlentz, G. *J. Am. Soc. Mass Spectrom.* **2006**, *17*, 139−150.
(58) Laiko, V. V.; Taranenko, N. I.; Berkout, V. D.; Yakshin, M. A.; Prasad, C. R.; Lee, H. S.; Doroshenko, V. M. *J. Am. Soc. Mass Spectrom.* **2002**, *13*, 354−361.

an $X-Y$ translation stage. The spatial resolution of such a system is defined by the focal diameter of the laser beam. For a simple long working distance lens and 337 nm light from a nitrogen laser this diameter is typically ~50 μm, although more sophisticated optical arrangements can achieve submicrometer spot sizes.[19] For analytes completely removed by the desorption process, Jurchen et al.[31] offered some improvement by oversampling. In this method the scanning step size is set smaller than the laser spot size and becomes the limiting factor that determines the spatial resolution.

Despite the growing success of MALDI-MS as a molecular imaging technique, two major obstacles stand in the way of its widespread application. First, mixing and cocrystallizing the sample with the light-absorbing matrix material can significantly obscure the original spatial distribution of analytes (e.g., through lateral mixing). Second, the need to transfer the sample into a vacuum environment for mass analysis considerably restricts the choice of samples. Both of these requirements for successful MALDI analysis exclude the possibility of in vivo measurements. The information on the spatial distributions and temporal variations of chemical species in biological systems is essential to understand metabolic pathways and, in general, complex biological processes.

In this contribution, we present a new approach to molecular imaging based on mid-IR laser excitation for AP-MALDI that mitigates both of these impediments. Molecular imaging of peptide distributions on surfaces and the distribution of various small molecules in biological tissue without the addition of a matrix are demonstrated.

EXPERIMENTAL SECTION

Mass Spectrometer and Laser. A Q-TOF Premier orthogonal acceleration time-of-flight (TOF) mass spectrometer (Waters Co., Milford, MA) was modified by replacing the electrospray source with a custom-made AP laser desorption ion source. The inlet capillary had a length of 30 mm and an internal diameter of 127 μm. The mid-IR output of a Nd:YAG laser-driven tunable optical parametric oscillator (OPO) (set to 2940 nm, 10 Hz) was projected onto the sample mounted on a stainless steel probe to produce the ions. The pulse duration of the laser was 4 ns. A single plano−convex focusing lens with 50 mm focal length produced an elliptical laser spot of ~250 μm average diameter. The incident angle of the laser beam was approximately 45°. The maximum energy of a laser pulse at the target was measured to be 150 μJ that translated into a fluence of 0.31 J/cm^2. This corresponds to a weak phase explosion regime.[59] The closest possible distance, ~2 mm, between the mass spectrometer inlet and the target surface was selected to maximize the ion signal but still avoid an electrical breakdown. All the experiments were performed in the positive ion mode.

Pulsed Dynamic Focusing. In order to improve the ion collection efficiency, pulsed dynamic focusing (PDF) was implemented.[60] In PDF when the ions in the expanding laser plume are sufficiently close to the mass spectrometer inlet, the extraction voltage is reduced to zero. Through the rest of the way to the inlet the ions are guided by the aerodynamic flow created by the suction of the orifice. Consistent with earlier results,[60] our experiments showed that, compared to a static electric extraction field, the PDF improved the ion collection efficiency by approximately a factor of 5.

There were several PDF and source parameters to optimize to achieve this improvement. These included the high voltage applied to the target plate, the temperature of the capillary, and the high-voltage pulse width. The best results were obtained at 3.0 kV target plate voltage held for 13 μs, 150 °C interface block temperature, and −50 V interface voltage.

Imaging. A stepper motor-driven three-axis precision flexure stage (NanoMax TS, Thorlabs, Newton, NJ) was computer controlled to scan the sample surface by laterally moving the target plate in front of the inlet orifice. The flexure stage with additional piezoelectric actuators and displacement sensors had a travel range of 4 mm and an ultimate resolution of 5 nm. Thus, the spatial resolution of the imaging experiment (except for the oversampling method) was limited by the focal spot size of the laser beam.

Mass spectra produced by up to 80 laser shots were averaged for each spot on the sample surface and stored as a function of time. A LabVIEW program that rendered the times to the corresponding $X-Y$ coordinates converted these datasets into two-dimensional distributions. A scientific graphics package (Origin 7.0, OriginLab Co., Northampton, MA) was used to produce false color images of the species distributions.

Materials and Sample Preparation. HPLC-grade triacetate salt of bradykinin, acetate salt hydrate of substance P, bovine insulin, and 2,5-dihydroxybenzoic acid (DHB), as well as reagent-grade reserpine, succinic acid, thiourea, and glycerol were purchased from Sigma-Aldrich. The aqueous 1% solution of toluidine blue O was obtained from Home Training Tools, Ltd. Both the analytes and the matrixes were used without further purification. Deionized water with 18.3 MΩ·cm resistivity was produced with an E-pure system (D4631, Barnstead, Dubuque, IA).

The conventional MALDI samples were produced by mixing 1 μL of the diluted 2×10^{-4} M peptide stock solution prepared in 0.01% TFA with 1 μL of the saturated matrix solution prepared in 70% (v/v) HPLC-grade aqueous acetonitrile solution. For crystalline matrixes, the samples were allowed to air-dry at room temperature.

Fresh strawberries, bananas, and grapes were purchased from a local supermarket. Sections of 0.2−0.5 mm in thickness were prepared at room temperature with a sharp utility knife. The tissue sections were quickly transferred onto the stainless steel probe without any pretreatment. The wet tissue sections adhered to the target surface with sufficient strength to hold them in place during the laser desorption and imaging experiments.

RESULTS AND DISCUSSION

Sensitivity and Interferences. Due to ion production, collection, and transport losses in the AP environment and within the interface itself, the AP-MALDI ion sources are perceived as less efficient than their vacuum counterparts. To test the utility of our AP-MALDI system, the sensitivity and spectral interferences were assessed. A series of dilution experiments using reserpine (m/z 608.7) and bradykinin (m/z 1060.4) analyte and saturated DHB matrix solutions showed that for the entire sample spot the sensitivity was 300 fmol, whereas in imaging experiments for individual pixels ~1 fmol/pixel sensitivity was achieved using S/N

(59) Chen, Z.; Bogaerts, A.; Vertes, A. *Appl. Phys. Lett.* **2006**, *89*, 041503.
(60) Tan, P. V.; Laiko, V. V.; Doroshenko, V. M. *Anal. Chem.* **2004**, *76*, 2462−2469.

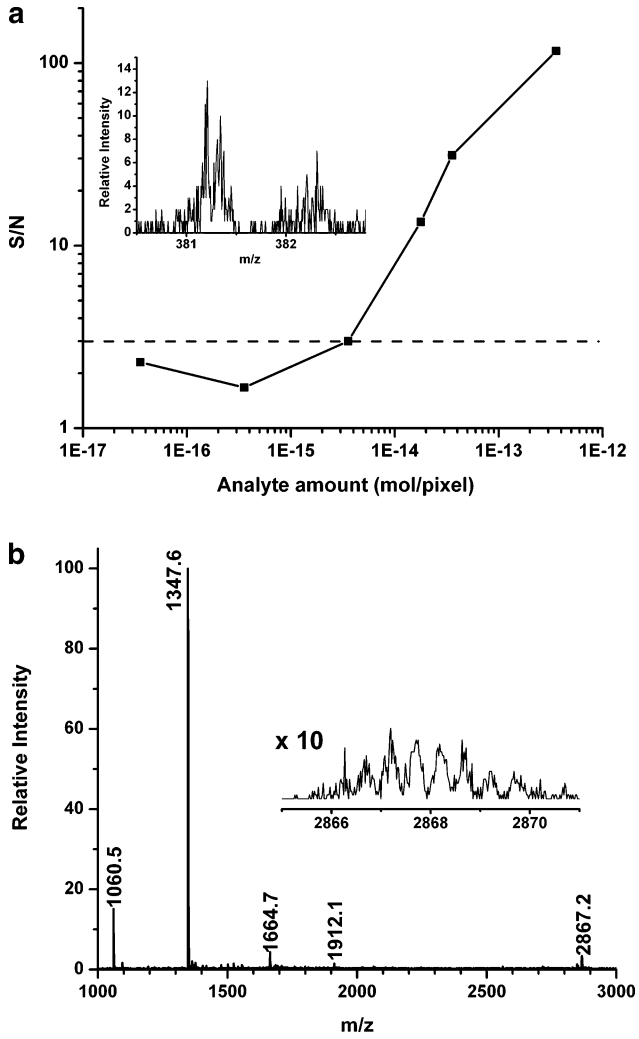

Figure 1. (a) Signal-to-noise ratio for potassiated sucrose ions (*m*/*z* 381.1) from aqueous matrix using AP IR-MALDI shows ~3 fmol/pixel detection limit. Inset shows the marginal signal at *m*/*z* 381 and its vicinity in the corresponding mass spectrum. (b) AP IR-MALDI mass spectrum of equimolar bradykinin (*m*/*z* 1060.4), substance P (*m*/*z* 1347.6), and bovine insulin (*m*/*z* 5733.5) mixture with DHB as a matrix. Bovine insulin ions are low in abundance and appear as doubly and triply charged species at *m*/*z* 2867.2 and 1912.1, respectively.

> 3 as the detection criterion. In the presence of potassium ions, somewhat higher detection limit, ~3 fmol/pixel, was found for the direct desorption of sucrose from aqueous environment. This system (with the use of a cold finger) was used to model the most abundant components in the fruits used in the imaging experiments (see below). Figure 1a shows the dependence of the signal-to-noise ratio (S/N) for the potassiated sucrose ions as a function of solution concentrations. At ~3 fmol/pixel the S/N drops below 3 and the signal becomes commensurate with the noise. The inset depicts the marginal signal at *m*/*z* 381 and its vicinity in the corresponding mass spectrum.

Both in the case of DHB and water as a matrix, matrix-related interferences were absent. This is consistent with the general notion of efficient matrix suppression in AP-MALDI reported in the literature.[39,61]

The sensitivity in our system also depended on the mass of the analyte. Figure 1b shows the AP IR-MALDI mass spectrum for an equimolar (100 pmol each) mixture of bradykinin, substance P (*m*/*z* 1347.6), and insulin (*m*/*z* 5733.5). While the bradykinin and substance P peaks were strong, no singly charged insulin signal was detected. The weak peaks at *m*/*z* 2867.2 and 1912.1 corresponded to the doubly and triply protonated forms of insulin, respectively. Although analyte suppression effects by the low-mass peptides could account for reduced insulin intensities, experiments with insulin alone confirmed that these observations were mostly due to the reduced sensitivity in the *m*/*z* > 3000 region.

For vacuum UV-MALDI and IR-MALDI, the typical sensitivity values are in the low femtomole and subpicomole range, respectively.[62] For ion trap instruments in AP UV-MALDI experiments absolute sensitivity values were reported at the low femtomole level.[38] Direct AP analysis of oligosaccharides with an IR laser from the solution phase also indicated femtomole sensitivity.[50] Thus, it seems, for AP-MALDI ion sources (including ours) the current challenge is not the absolute sensitivity for the best case compounds but the demonstration of consistent analytical performance for broad classes of molecules.

Further improvements in the sensitivity of the AP-MALDI interface can be expected from enhancing the production, collection, and transport of ions. Ion yields in AP laser−solid interactions depend on laser wavelength, pulse duration, beam diameter, incident angle, and fluence. Ion collection and transport under AP conditions depend on the potential distributions and the aerodynamics of the interface. Key parameters include the inlet orifice geometry, the distance between the inlet and the target surface, the position of the laser spot on the target surface with respect to the inlet orifice, the applied voltages, temperature distributions, and the auxiliary gas flow. As the AP ion sources have a shorter history than their vacuum counterparts, unexplored new arrangements can offer substantial benefits. Vice versa, we found that the off-axis displacement of the laser spot with respect to the mass spectrometer inlet by 1 mm reduced the signal by approximately 1 order of magnitude. Similar sharp dependence on gas flow conditions was described in the literature.[63]

Molecular Imaging of Mock Peptide Distributions. Several known IR matrixes, including DHB, succinic acid, thiourea, glycerol, and water, were tested in AP laser desorption experiments. Although all of these matrixes produced analyte ion signal, for the small peptides studied, DHB and water offered the strongest peaks and the best signal-to-noise ratio.

Encouraged by the robust AP-MALDI signal, imaging experiments on mock peptide distributions were performed. Figure 2 shows the molecular images of the three characters in the word "ION", with the intensity of substance P at *m*/*z* 1347.6 represented on a false color scale. In these experiments, 1 μL of the analyte DHB mixture was transferred onto the target plate and allowed to air-dry. An adhesive paper mask with the letters "I", "O", and "N" excised was attached to the sample surface. As our flexure stage had a range of 4 mm in the *X* and *Y* directions, scanning of the surface was performed one character at a time. Because the focal spot of our IR laser was 250 μm, initially a 125 μm scanning

(61) Moyer, S. C.; Marzilli, L. A.; Woods, A. S.; Laiko, V. V.; Doroshenko, V. M.; Cotter, R. J. *J. Int. Mass Spectrom.* **2003**, *226*, 133−150.

(62) Kirpekar, F.; Berkenkamp, S.; Hillenkamp, F. *Anal. Chem.* **1999**, *71*, 2334−2339.

(63) Miller, C. A.; Yi, D. H.; Perkins, P. D. *Rapid Commun. Mass Spectrom.* **2003**, *17*, 860−868.

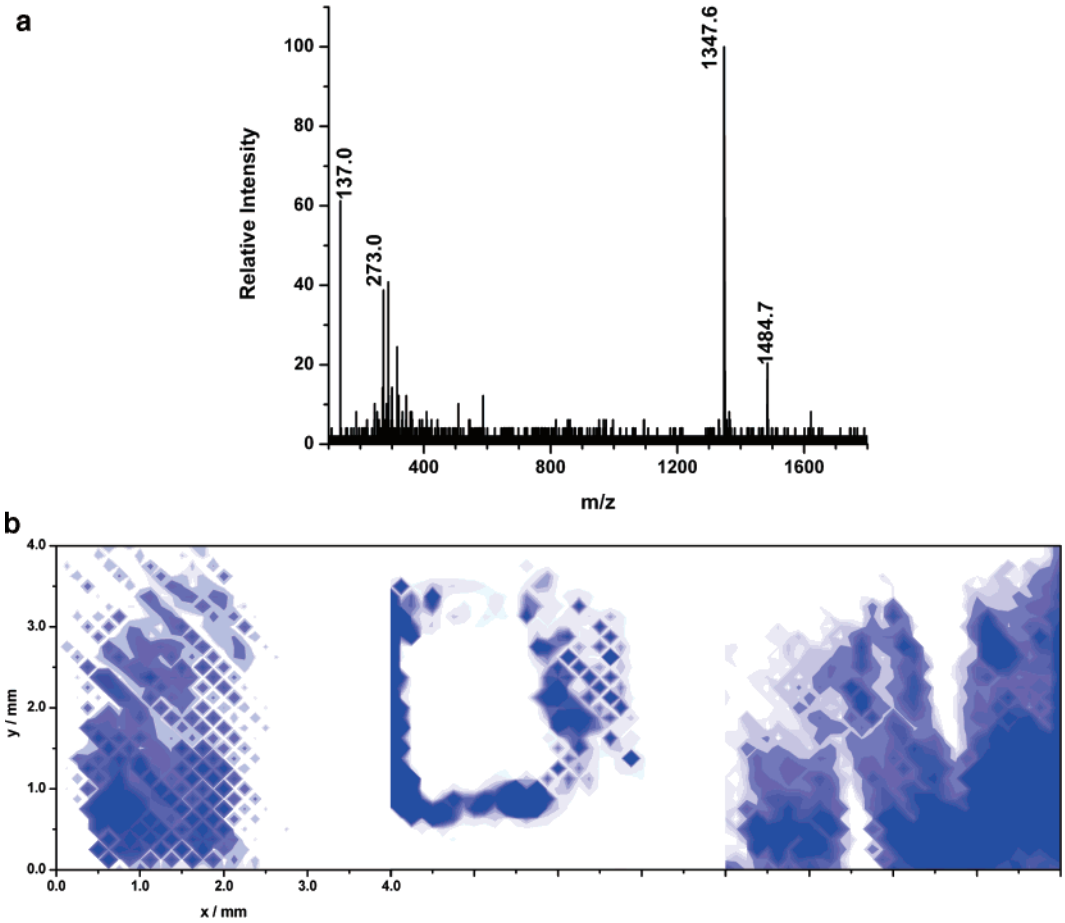

Figure 2. (a) AP IR-MALDI mass spectrum of substance P from DHB matrix based on 10 laser shots. (b) Molecular image of the three characters in the word "ION" at *m*/*z* 1347.6 corresponding to the substance P molecular ion. The characters were created by a paper mask over the sample surface. The scanning step size and the dwell time were 125 μm and 8 s/pixel, respectively.

step size was selected. Although spectral features were already discernible after 1 s (10 laser shots), to achieve high signal-to-noise ratio, each surface position was interrogated for 8 s and the spectra from the 80 laser shots were averaged.

Figure 2a displays a mass spectrum obtained by averaging the signal for 10 laser shots. The base peak at m/z 1347.6 corresponds to substance P. It is accompanied by the dehydroxylated DHB fragment ion at m/z 137.0 and by its adducts with a substance P molecule at m/z 1484.7 and with a neutralized DHB fragment at m/z 273.0. To determine the substance P distribution over the surface, the m/z 1347.6 peaks were integrated for every position of the translation stage, the corresponding pixels were colored according to the peak areas and mapped to the surface to produce an image (see Figure 2b). Although the original pattern and the three characters are clearly discernible, due to the uneven mask surface and probably to the charging of the insulating paper mask during the experiments the image in Figure 2b is fairly crude. We estimated the spatial resolution to be ~200 μm on the basis of the measurement of the size differences between the actual and imaged patterns. This, in part, is attributed to the rudimentary method of producing the distribution and to the inherent limitation on the spatial resolution imposed by the size of the laser focal spot.

The focusing of the laser beam in our system is limited by the optical arrangement to ~250 μm. Significant improvement can be expected from optics with higher numerical aperture. Short of complex designs and precision optical components this cannot be achieved with the long working distance (~5 cm) necessary to accommodate the sample inlet of our mass spectrometer. Thus, in order to improve the spatial resolution, we implemented the oversampling technique described by Jurchen et al. for vacuum UV-MALDI imaging.[31] This method can only be used if the analyte is largely depleted in every interrogated point. By moving the translation stage to the next point with an increment smaller than the laser spot size, fresh sample surface is exposed. Collecting mass spectra from these partially fresh areas provides a spatial resolution limited by the step size of the translation stage.

The left panel in Figure 3a shows the optical image of the electron microscope grid with 92 μm bar spacing used as a mask to cover a homogeneous toluidine blue surface. The created pattern was imaged by AP IR-MALDI with oversampling at a 40 μm step size (see the right panel in Figure 3a). In order to deplete the sample in a particular point a dwell time of 8 s was selected for each pixel. The image was constructed using the m/z 270.1 base peak representing the organic cation from the toluidine blue O salt. In Figure 3a the pattern created by the grid is clearly seen. Figure 3b corresponds to an ion intensity profile perpendicular to the grid bars. To get a rough estimate of the spatial resolution, we determined the distance along the profile for which the ion intensity increased from 20% to 80% of the maximum value.[14,32] By this definition, the spatial resolution in Figure 3b was ~40 μm, approximately 5−6 times better than what was obtained with the

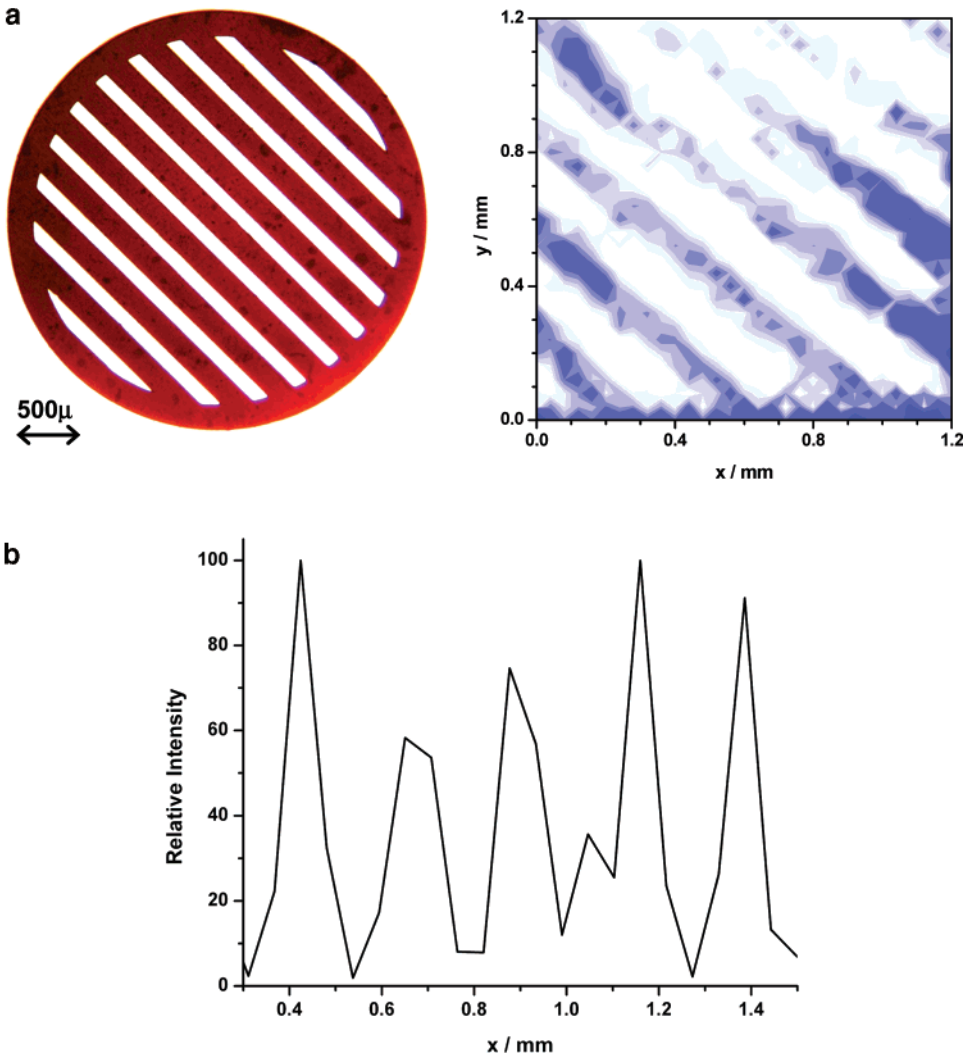

Figure 3. (a) Left panel: optical image of the electron microscope grid used as a mask to create chemical contrast with 92 μm features (gap width). Right panel: AP IR-MALDI molecular image of toluidine blue O in the exposed areas under the grid based on the *m*/*z* 270.1 ion obtained using the "oversampling" method. (b) Averaged ion intensity profile perpendicular to the grid bars indicated a lateral resolution of 40 μm.

limitation imposed by the laser spot size. As the smallest imaged details of the sample, the 92 μm gaps, were smaller than the diameter of the laser spot, these results clearly indicated the power of oversampling, i.e., without oversampling no features could be distinguished in this image.

It is interesting to note that oversampling is more likely to work with IR—than with UV—MALDI. It is known that the thickness of removed material for DHB in IR-MALDI is at least 10 times larger than in UV-MALDI.[64] Thus, the condition of largely depleted spots is easier to achieve with the IR laser. Indeed, for most of the samples in this study, the analyte ion signal decreased significantly upon multiple laser exposure of the same spot. Typically, after 50 laser shots, the signal intensity dropped by at least 1 order of magnitude.

Liquid Matrixes. Recent studies indicated the benefits of liquid matrixes, e.g., water and glycerol, in the AP laser desorption MS of peptides.[58,65,66] In comparison to solid matrixes these benefits include simplified sample handling, a vastly expanded array of applications, better shot-to-shot reproducibility, and the potential for better quantitation. Furthermore, liquid water is the natural matrix of cells, tissues, and other biological systems. Thus, successful AP IR-MALDI from liquid matrixes is a prerequisite for molecular imaging of biological tissues at atmospheric conditions. The obvious benefits of liquid matrixes are accompanied by some complications. Water, the most attractive liquid matrix in the IR, is fairly volatile, especially under the high gas flow, high thermal load conditions of the AP ion source. Also for both water and glycerol, Laiko et al.[58] observed that the ion formation took place only at the droplet contact line area closest to the direction of the laser beam.

To clarify these issues we revisited the utility of water—glycerol systems as matrixes for AP IR-MALDI. Ion yields of substance P analyte were monitored using four water—glycerol matrix systems, containing 100%, 70%, 50%, and 0% (v/v) glycerol. Under identical conditions pure glycerol and pure water produce the weakest and

(64) Kampmeier, J.; Dreisewerd, K.; Schurenberg, M.; Strupat, K. *Int. J. Mass Spectrom. Ion Processes* **1997**, *169*, 31—41.
(65) Coon, J. J.; Steele, H. A.; Laipis, P. J.; Harrison, W. W. *J. Mass Spectrom.* **2002**, *37*, 1163—1167.
(66) Turney, K.; Harrison, W. W. *Rapid Commun. Mass Spectrom.* **2004**, *18*, 629—635.

Table 1. Average Concentrations of Major Chemical Constituents in Strawberries, Bananas, and Grapes

	concentrations (% w/w)			
constituents	strawberries (stems removed)[a]	strawberries Oso Grande[b]	bananas (skin removed)[a]	grapes Thompson seedless[a]
water	90.95 ± 0.21	90.5 ± 0.3	74.91 ± 0.29	80.54 ± 0.41
glucose	2.04 ± 0.24	1.71 ± 0.02	4.98 ± 0.81	7.20 ± 0.10
fructose	2.50 ± 0.24	1.93 ± 0.04	4.85 ± 0.66	8.13 ± 0.22
sucrose	0.12 ± 0.06	1.80 ± 0.07	2.39 ± 0.55	0.15
starch	0.04 ± 0.03		5.38 ± 0.55	0.00
citric acid		0.59		
potassium	0.153 ± 0.004		0.358 ± 0.002	0.191 ± 0.006
sodium	0.001 ± 0.0001		0.001 ± 0.0004	0.002 ± 0.0003

[a] USDA—National Agricultural Lab: http://www.nal.usda.gov (ref 71). [b] Ref 68.

the strongest analyte ion signal, respectively, whereas the ions from the 70% and 50% glycerol solutions exhibit similar intermediate abundances. The sample based on pure water, however, rapidly evaporated allowing only 1−2 min for data acquisition.

Two methods were tested to prolong the period of ion production without compromising the analyte ion intensity. In the first method, the aqueous sample solution was carefully layered on top of a thin glycerol film (1 μL) coating the probe. Care was taken to minimize mechanical mixing of the two layers. This method gave a stable analyte signal lasting for over 30 min, and the signal intensity was comparable to that obtained using pure water. Similar to earlier observations,[58] for pure glycerol and glycerol/water mixtures we also observed ion formation primarily in the droplet contact line area facing the laser beam. However, for the layered samples, ions were found to be efficiently generated from any position on the sample surface. Thus, by producing sustained ion signal and location independent ion yields, these layered samples alleviated two of the difficulties associated with liquid matrixes.

A second method to prolong the ion signal from liquid samples was the cooling of the stainless steel target plate. Instead of the thermoelectric cooling based on a Peltier device described in the literature,[67] we used the target as a cold finger. First the sample solution was transferred to the target plate, then it was immersed into either liquid nitrogen or dry ice. After 2−3 min, the target plate was sufficiently cold to keep the sample from rapidly evaporating. It was visually observed in the experiments that the first 500−600 laser shots thawed the surface layer of the frozen sample, but the reduced temperature of this solution due to the cooling effect of the still frozen bulk of the sample enabled data acquisition for over 15 min. It should be pointed out that, unlike in some early IR-MALDI studies,[52] in the experiments described above it is liquid water rather than ice that serves as a matrix.

Plant Tissue Analysis without External Matrix. Water is a native component of biological samples. In particular, plants, especially fruits, are rich in water. On the basis of our experience with water as a matrix, AP IR-MALDI experiments were conducted on fruit tissue sections. Table 1 lists the average concentrations of the major chemical constituents in strawberries, grapes, and bananas. The water concentrations for the three fruits listed in Table 1 range from 75 wt % (bananas) to 91 wt % (strawberries). Indeed, the laser energy was efficiently coupled into these tissues and mass spectra were generated. The dominant water-soluble components are glucose, fructose, sucrose, citric acid, and potassium ions.

The averaged mass spectra from 300 laser shots fired at randomly selected points on the three fruit tissues are shown in Figure 4. The base peak for strawberries and bananas at m/z 381.1 and the second largest peak for grapes was assigned as the potassiated sucrose ion, $[Glc\alpha(1-4)\beta Fru + K]^+$. Ionized clusters of sucrose were also observed at m/z 723.2, 1065.3, and 1407.4 corresponding to $[2(Glc\alpha(1-4)\beta Fru) + K]^+$, $[3(Glc\alpha(1-4)\beta Fru) + K]^+$, and $[4(Glc\alpha(1-4)\beta Fru) + K]^+$, respectively. The inset in Figure 4a shows the isotope pattern for the m/z 219.0 (see later) and 381.1 ions. The isotope peak intensity distributions for both ions are consistent with the presence of potassium, i.e., they have an elevated level of $[Glc\alpha(1-4)\beta Fru + K + 2]^+$, indicating the contribution of the ^{41}K isotope. In all three spectra the m/z 365.1 peak is present, and it can be identified as the sodiated form of sucrose, $[Glc\alpha(1-4)\beta Fru + Na]^+$. The abundance of these ions is much lower than the potassiated counterparts, consistent with the higher concentration of potassium than sodium in the three fruits (for example in strawberries, according to Table 1, the molar concentration of potassium is about 90 times higher than that of sodium).

The base peak for grapes and the second largest peak for strawberries and bananas is at m/z 219.0. This ion can be assigned as a potassiated glucose or fructose, $[Glc/Fru + K]^+$. The presence of potassium in this ion is corroborated by the corresponding isotope distribution shown in the inset of Figure 4a. Unlike in electron impact mass spectra where small differences in the fragmentation pattern exist, in MALDI the structural isomers, glucose and fructose, cannot be distinguished. On the basis of the information in Table 1, it is expected that this peak has contributions from the potassiated form of both monosaccharides. In bananas potassiated mixed clusters of glucose/fructose and sucrose, $[Glc/Fru + Glc\alpha(1-4)\beta Fru + K]^+$ and $[Glc/Fru + 2(Glc\alpha(1-4)\beta Fru) + K]^+$, were also observed at m/z 561.1 and 903.3, respectively. In all three spectra a strong peak appears at m/z 399.1. It can be assigned as a water adduct of the potassiated sucrose ion, $[Glc\alpha(1-4)\beta Fru + H_2O + K]^+$. In the mass spectrum of strawberry, the medium abundance m/z 231.0 ion was assigned as potassiated citric acid. Table 1 indicates that strawberries, indeed, contain ~0.6% citric acid. The assignment of several other

(67) Von Seggern, C. E.; Gardner, B. D.; Cotter, R. J. *Anal. Chem.* **2004**, *76*, 5887−5893.

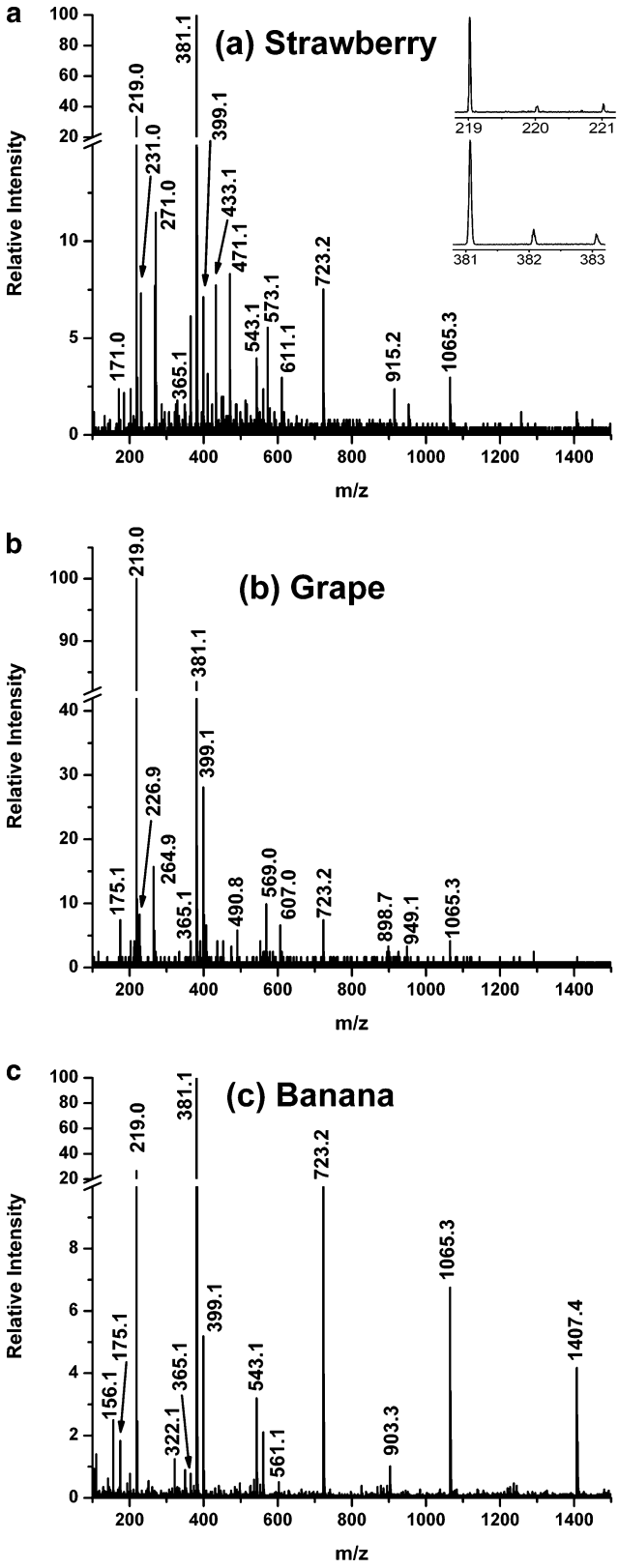

Figure 4. Mass spectra of (a) strawberry, (b) grape, and (c) banana, in which the ions with *m*/*z* 381.1 are assigned as the potassiated sucrose ion. The ions observed at *m*/*z* 723.2, 1065.3, and 1407.4 correspond to $[2(\text{Glc}\alpha(1-4)\beta\text{Fru}) + \text{K}]^+$, $[3(\text{Glc}\alpha(1-4)\beta\text{Fru}) + \text{K}]^+$, and $[4(\text{Glc}\alpha(1-4)\beta\text{Fru}) + \text{K}]^+$. At *m*/*z* 219.0 a strong peak appeared indicating potassiated Glc/Fru in the sample. In bananas potassiated mixed clusters of glucose/fructose and sucrose, $[\text{Glc/Fru} + \text{Glc}\alpha(1-4)\beta\text{Fru} + \text{K}]^+$ and $[\text{Glc/Fru} + 2(\text{Glc}\alpha(1-4)\beta\text{Fru}) + \text{K}]^+$, were also observed at *m*/*z* 561.1 and 903.3, respectively.

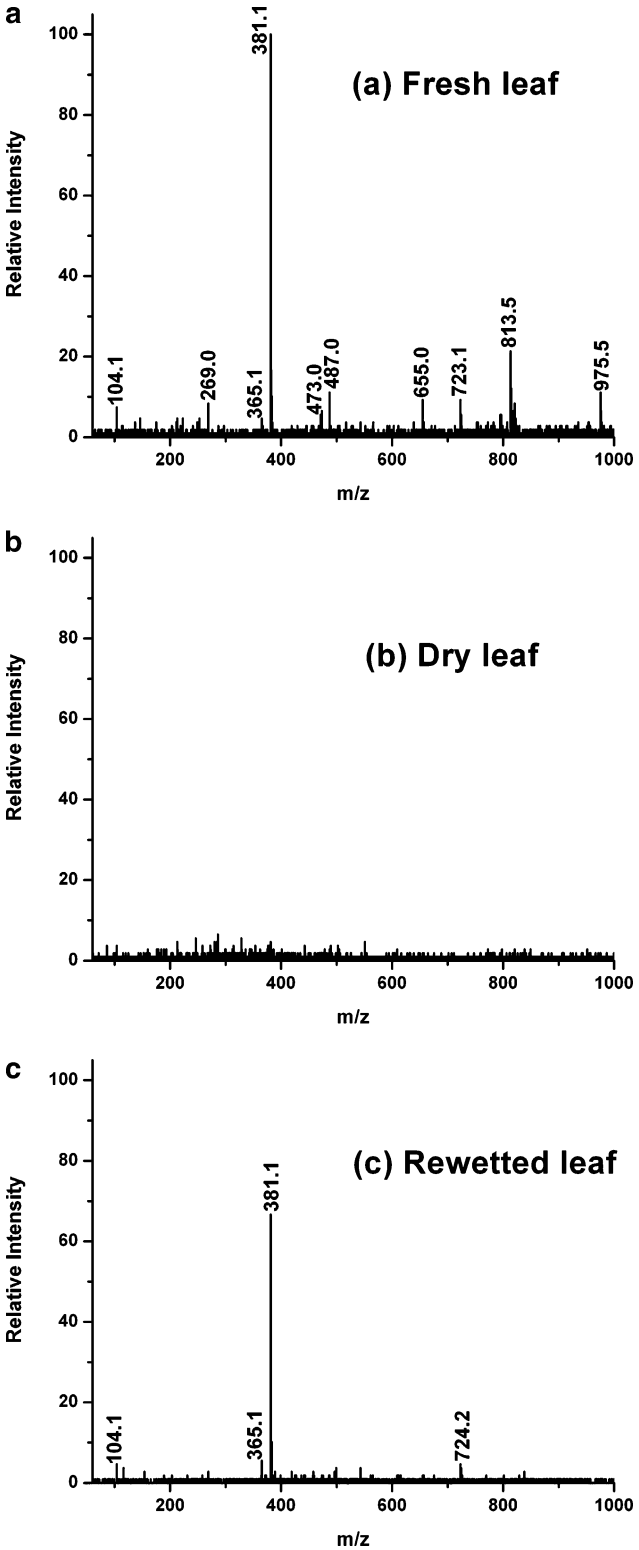

Figure 5. Mass spectra of a (a) fresh, (b) air-dried, and (c) rewetted rose leaf section exhibit potassiated sucrose and smaller unidentified peaks. Upon drying the leaves, the ion signal disappeared, whereas rewetting restored some of the signal. These results point to the essential role of native water in AP IR-MALDI.

ions that appeared in the spectra of strawberries and bananas but not in grapes, such as *m*/*z* 175.1 and 543.1, requires additional work. These variations are potentially related to the actual concentration changes of these species within the tissue. Our

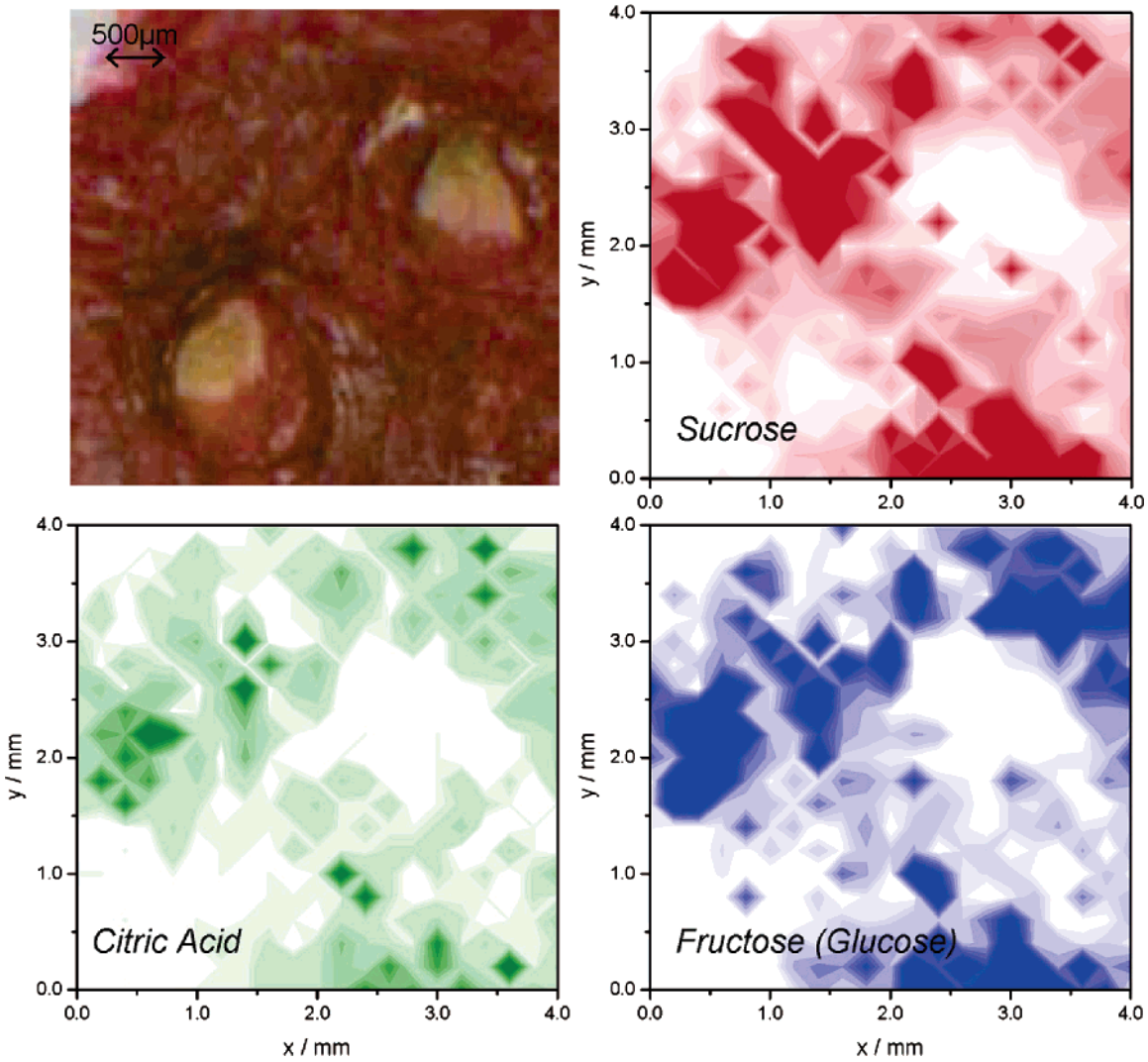

Figure 6. Optical image of a strawberry skin (top left) compared to AP IR-MALDI images for three major components, sucrose (top right), glucose/fructose (bottom right), and citric acid (bottom left) around embedded seeds. The false color intensities were assigned according to integrated areas of the associated potassiated peaks. Although the distributions of these water-soluble components are similar, the position of the two seeds, with lower concentrations of these compounds, is clearly discernible.

ability to identify soluble saccharides and organic acids directly from plant tissue is important because they are central metabolites in glycolysis, the citric acid cycle, and other metabolic pathways.

Other known components in strawberries, such as ascorbic acid (0.06 wt %), anthocyanins (0.04 wt %), flavonols, ellagic acid (0.002 wt %), and phenolics usually present at significantly lower concentrations were not identified.[68] The percentages in parentheses relate to the Oso Grande cultivar. At this stage it is hard to decide why these components are not identified in the spectra. There are many possible explanations, including localization of these constituents in other parts of the fruit, signal suppression effect by the main components, and less than ideal ionization or ion extraction conditions for them in the laser plume.

To test the utility of AP IR-MALDI for the analysis of other plant tissues freshly cut rose leaves, leaves air-dried for 48 h, and samples rewetted in water (soaked in deionized water for 30 s) were analyzed without any sample preparation. The normalized mass spectra are shown in Figure 5. Similar to our results with fruits, the potassiated sucrose ion at m/z 381.1 dominates the mass spectra. For fresh leaves a series of smaller peaks also appear at m/z 487.0, 655.0, 813.5, and 975.5. Only marginal signal was observed for the dry leaves, whereas the rewetted leaves gave just slightly weaker sucrose peak than the fresh one. Most of the small peaks observed for the fresh leaves however did not reappear after rewetting the dried ones. This might be an indication that those peaks were associated with volatile components in the leaves and/or resulted from the differences in the efficacy of native and external water as a matrix. The lack of ion signal from the dried leaves also indicated the critical role water played in the AP IR-MALDI process.

Molecular Imaging of Plant Tissue. On the basis of the robust signal from the main components in the studied fruits, low-resolution imaging experiments were performed on strawberry skin tissue. To complete the imaging in less than 30 min, a 21 × 21 pixel array was used with a 4 s/pixel dwell time and a 200 μm step size. It was found that longer scanning time led to significant dehydration of the sample, resulting in decreased signal intensity and skewed component distributions. To introduce chemical

(68) Cordenunsi, B. R.; Do Nascimento, J. R. O.; Genovese, M. I.; Lajolo, F. M. *J. Agric. Food Chem.* **2002**, *50*, 2581−2586.

heterogeneity, the field of view was selected to include some seeds.

Together with the optical image, the distribution of the potassiated sucrose, $[Glc\alpha(1-4)\beta Fru + H_2O + K]^+$, glucose and/or fructose, $[Glc/Fru + K]^+$, and citric acid are shown in Figure 6. Although the distributions of these water-soluble components are similar, the position of the two seeds, with lower concentrations of these compounds, is clearly discernible. The signal in the seed region was marginal and did not allow the identification of the chemical components present. As the scanning step size of 200 μm was comparable to the dimensions of the seeds their shape is not reflected accurately in the molecular images. Nevertheless the information on the spatial distribution of these small metabolites can be useful in exploring biosynthesis and metabolic pathways in plants. For example, sucrose is the major form of transport for photoassimilated carbon and is both a source of the carbon skeletons and energy for plant organs unable to perform photosynthesis (sink organs).

The ability to perform AP IR-MALDI using native water as the matrix enables the in vivo investigation of the spatial distributions and temporal variations of chemical components in plant and animal tissues. The current limitations on the step size are not fundamental as both the laser focal spot and the translation stage step size can be reduced. Drying of the tissue during data acquisition can be mitigated by using a higher repetition rate laser and by providing an environment of controlled humidity, for example in an environmental chamber, for the analysis. Spatial correlations of unknown constituents can be used in deciphering their role in the organism.[69]

Our current understanding of the AP IR-MALDI ablation process points to some potential limitations in analytical performance. The interaction of mid-IR Q-switched laser radiation with water-rich targets, such as sections of soft tissues, exhibits two major phases.[70] In the first phase lasting for ~1 μs, a hot plume is created through surface evaporation and phase explosion. This plume exhibits strong shock waves[59] and is decelerated and eventually stopped by the background gas pressure. In the second phase lasting up to tens of microseconds, the recoil pressure expels additional material in the form of liquid droplets. The analytically useful information stems from the initial plume because it produces the ions for analysis, whereas the secondary material ejection can be considered detrimental as it leads to spot-to-spot cross contamination. Therefore, in order to optimize the analytical performance one has to achieve high ion yields in the first phase and minimize material ejection in the second. This can be achieved by finding a tradeoff in laser fluence that is high enough to produce ions for analysis but sufficiently low to minimize cross contamination.

CONCLUSIONS

Molecular imaging with MALDI mass spectrometry is a rapidly developing field. Most imaging work in the literature focuses on UV-MALDI imaging in vacuum environment with the help of an external matrix overlayer. In this contribution our first results with AP IR-MALDI are described that enable imaging at atmospheric pressure without the addition of an artificial matrix. Instead, the native water content of the biological tissue is utilized as an energy absorbing matrix.

The results are encouraging as the major water-soluble components in various fruits have been detected, identified, and their molecular distributions were imaged. It is essential, however, to explore if components with lower concentration and/or water-insoluble molecules are amenable for AP IR-MALDI. On the basis of studies in artificial matrixes, the sensitivity of our interface and mass spectrometer was verified at the ~1 fmol/pixel level. This indicates that the instrument is capable of detecting trace constituents of a sample.

An important limitation of UV-MALDI imaging in vacuum environment is the reduced amount of information in the low mass (m/z < 1000) region. Due to matrix interferences, this limitation becomes most apparent in the m/z < 500 domain. This might present a serious impediment in its application to following low molecular components, such as amino acids, organic acids, and saccharides, in metabolomics studies. The AP IR-MALDI approach readily generates information on many of these components in the low-mass range. Thus, it can be viewed as a complementary technique to UV-MALDI in molecular imaging experiments potentially useful for metabolomics applications.

As water is a native component of plant and animal tissues, the ability to perform AP IR-MALDI using water as the matrix enables the in vivo investigation of complex biological systems in their natural state. The damage inflicted on the tissue during imaging experiments is superficial (a few micrometers in depth); thus, larger organisms (e.g., plants) can survive the imaging experiments. Improvements in focusing and instrumental sensitivity can further enhance the applicability of this method for in vivo investigations by minimizing this damage.

By more sophisticated conventional focusing, higher spatial resolution can be achieved up to the diffraction limit. This requires beam expansion to reduce divergence and higher numerical aperture optics with a tighter focal spot. To sample surface areas below the diffraction limit (e.g., < ~1.5 μm for 3.0 μm radiation), near-field optics can be used. By launching the laser light into an optical fiber and moving the fiber tip sufficiently close to the target, the illuminated area becomes limited by the sharpness of the fiber tip. Typical optical fibers can be etched to a sharpness of ~100 nm. To take advantage of the corresponding extremely small probe volumes, further improvement in AP interfaces and mass spectrometric sensitivity are necessary.

ACKNOWLEDGMENT

The authors are grateful for the support of this work by the W. M. Keck Foundation (041904), the U.S. Department of Energy (DEFG02-01ER15129), and the George Washington University Research Enhancement Fund. Modified capillary inlets for this research were kindly provided by D. Kenny and the Waters Co.

Received for review August 23, 2006. Accepted November 8, 2006.

AC061577N

(69) Li, Y.; Shrestha, B.; Vertes, A. Proceedings of the 54th ASMS Conference on Mass Spectrometry and Allied Topics, Seattle, WA, May 28–June 1, 2006; DVD-ROM.

(70) Apitz, I.; Vogel, A. *Appl. Phys. A: Mater. Sci. Process.* **2005**, *81*, 329–338.

(71) See the USDA National Nutrient Database for Standard Reference at http://www.nal.usda.gov. (Accessed June 21, 2006).